FIRST LASING OF THE *LCLS* X-RAY FEL AT 1.5 Å

P. Emma, for the *LCLS* Commissioning Team; *SLAC*, *Stanford*, CA 94309, USA

Abstract

The Linac Coherent Light Source (*LCLS*) is a SASE 1.5-15 Å x-ray Free-Electron Laser (FEL) facility under construction at SLAC [1], and presently in an advanced phase of commissioning. The injector, linac, and new bunch compressors were commissioned in 2007 [2] and 2008 [3], establishing the necessary electron beam brightness at 14 GeV. The final phase of commissioning, including the FEL undulator and the long transport line from the linac, began in November 2008, with first 1.5-Å FEL light and saturation observed in mid-April 2009. We report on the accelerator, undulator, and FEL operations, although prior to the availability of the full x-ray diagnostics suite, which will not be ready until June 2009.

INTRODUCTION

First electrons were taken through the undulator channel on Dec. 13, 2008, requiring only two shots to be transported 200 m through the small 5-mm undulator chamber and to the main dump. No undulators were installed then, in order to protect the permanent magnets from unnecessary radiation. Twenty-one 3.4-m long undulator magnets were installed in late March and after just 3 days of system checkout, first 1.5-Å FEL light was observed on April 10, 2009. Design and typical measured parameters are listed in Table 1, including beam stability. The commissioning schedule is shown in Figure 1.

Table 1: Design and typical measured parameters. Stability values are taken over a few minutes and measured at 13.6 GeV.

Parameter	sym.	dsgn	meas.	unit
Bunch charge	Q	1	0.25	nC
Final linac e^- energy	γmc^2	13.6	13.6	GeV
FEL 3-D gain length	L_G	4.5	~3.3	m
Photons per pulse	N_γ	1	~0.8	10^{12}
Init. bunch length (rms)	σ_{z0}	0.9	0.65	mm
Final bunch length (rms)	σ_{zf}	20	6-8	μm
Final peak current	I_{pk}	3.4	3.0	kA
Proj. emittance (injector)	$\gamma\varepsilon_{x,y}$	1.2	0.4-0.7	μm
Slice emittance (injector)	$\gamma\varepsilon^s_{x,y}$	1.0	0.3-0.4	μm
Proj. emittance (14 GeV)	$\gamma\varepsilon^L_{x,y}$	1.5	0.5-1.6	μm
Single bunch rep. rate	f	120	10-30	Hz
RF gun field at cathode	E_g	120	115	MV/m
UV laser energy on cath.	u_l	250	12	μJ
UV laser diam. on cath.	$2R$	1.5	1.2	mm
Cathode quantum eff.	QE	6	10	10^{-5}
e^- energy stability (rms)	$\Delta E/E$	0.1	0.04	%
e^- x,y stability (rms)	x/σ_x	10,10	15,10	%
e^- timing stability (rms)	Δt	120	50	fs
Peak current stab. (rms)	$\Delta I/I$	12	9	%
Charge stability (rms)	$\Delta Q/Q$	2	2.5	%

At present (May '09) there are 25 (of 33) 3.4-m long undulator magnets installed and the x-ray diagnostics hall is not ready for x-rays until June. However, a simple YAG screen x-ray diagnostic, placed just 50 m after the undulator, has been used to estimate FEL power, with a preliminary gain length measurement of 3.0±0.3 m at 1.5 Å (13.64 GeV, see Table 1).

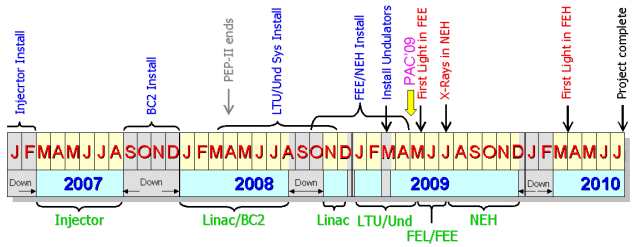

Figure 1: *LCLS* commissioning and installation schedule (2007-2010). Commissioning blocks are in green text, installation in blue, and project milestones in red. Down-time blocks are gray.

DRIVE LASER, GUN, AND INJECTOR

The UV drive laser system continues to perform well with >98% uptime. Spatial shaping is accomplished with an over-filled iris imaged to the cathode with a 1.2-mm diameter and temporal shaping is done using a *Dazzler*. The shaping quality can vary from week to week but routine maintenance and occasional replacement of damaged optics usually restores the UV shape.

The copper cathode has been replaced only once, in July 2008, after laser cleaning was used to increase the quantum efficiency (*QE*), leaving poor uniformity. The UV spot is intentionally offset transversely with respect to the solenoid field center in order to produce the highest *QE* and smallest time-sliced emittance. Offsets of 1 mm do not appear to be detrimental to the emittance.

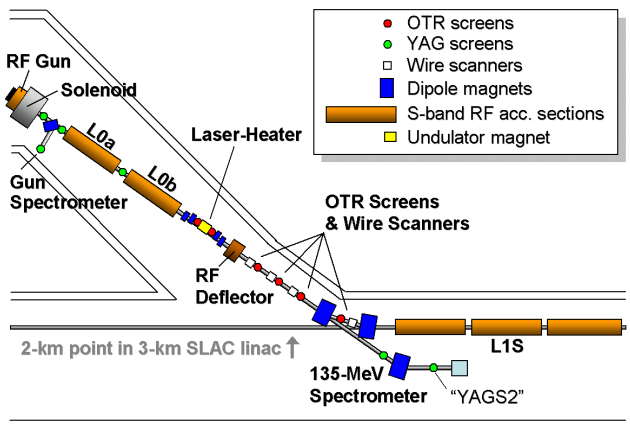

Figure 2: Injector layout showing gun, laser heater, 1 transverse RF deflector, screens, wire scanners, and spectrometers.

The thermal emittance (horizontal only) has been measured several times with the 'new' cathode using very low charge (20 pC) and time-slicing the bunch using the transverse RF deflector [4] (Figure 2) with values down to $\gamma\varepsilon_x \approx 0.24$ µm with a 1.2-mm laser spot diameter and $\gamma\varepsilon_x \approx 0.12$ µm with a 0.6-mm diameter. These very low

emittance values have initiated a study of the possibilities of running the *LCLS* at just 20 pC, suggesting a 2-fs x-ray pulse is possible with nearly 10^{12} photons per pulse [5].

The bunch charge is normally held at 0.25 nC during most of the commissioning, which improves linac emittance preservation and beam stability. A projected emittance measurement at 135 MeV is shown in Figure 3 with 0.43 and 0.46 *x* and *y* emittance values at 0.25 nC (33 A), which are not uncommon. Some time has been spent with higher charge, up to 1 nC, but beam brightness and stability favors a lower charge, as had been anticipated [6]. Studies with higher and lower charge levels will be pursued after the main task of commissioning the many new systems is complete.

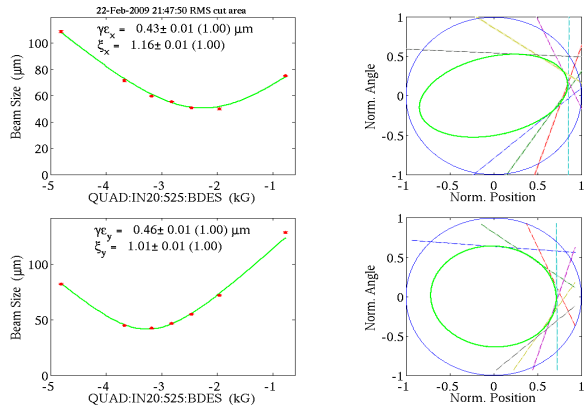

Figure 3: Projected *x* & *y* emittance measured on OTR screen after heater at 135 MeV, 0.25 nC ($\gamma\varepsilon_x \approx 0.43$ μm, $\gamma\varepsilon_y \approx 0.46$ μm).

LASER HEATER

The laser heater system [7] is located in the injector at 135 MeV (see Figure 2) and was fully installed and tested in the fall of 2008. This unique component is used to add a small level of intrinsic energy spread to the electron beam in order to Landau damp the micro-bunching instability before it potentially breaks up the high brightness electron beam. The laser heater system is composed of a 4-dipole chicane; a 9-period, planar, permanent-magnet, adjustable-gap undulator at the center of the chicane; one OTR screen on each side of the undulator for electron/laser spatial alignment; and an IR laser (≤15 MW) which co-propagates with the electron beam inside the undulator generating a 758-nm energy modulation along the bunch. The final two dipoles of the 4-dipole chicane time-smear this modulation leaving only a thermal-like intrinsic energy spread within the bunch.

Figure 4 shows the time-resolved energy spread measured on a YAG screen ("YAGS2" in Figure 2) for three different IR-laser pulse energy settings (0, 40 μJ, and 230 μJ). The transverse RF deflector [4] (Figure 2) is switched on here converting the vertical axis to time (the bunch length coordinate), while the 135-MeV spectrometer bend (see also Figure 2) converts the horizontal axis to energy, revealing longitudinal phase space and clearly demonstrating the intrinsic energy spread is increased with the IR laser. Table 2 lists the various parameters of the laser heater system.

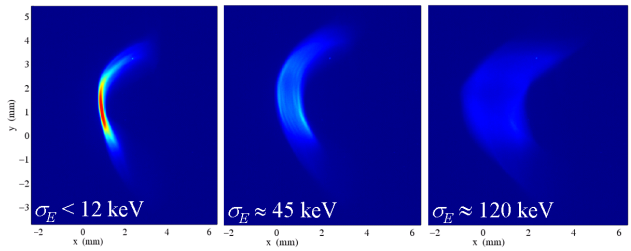

Figure 4: Measured time-sliced energy spread on "YAGS2" screen (see Figure 2) at 135 MeV with laser heater OFF (left), IR laser energy at 40 μJ (center), and again at 230 μJ (right). The rms energy spread values above agree with calculations.

Table 2: Laser Heater (LH) Parameters at 135 MeV & 0.25 nC.

Parameter	sym.	value	unit
LH-undulator parameter (adjustable)	K	1.38	-
LH-undulator period	λ_u	5.4	cm
No. of full LH-undulator periods	N_p	9	-
LH-undulator full gap (adjustable)	g_u	34.5	mm
IR laser wavelength	λ_{IR}	758	nm
IR laser pulse duration (FWHM)	Δt_{IR}	15	ps
Hor. offset at center of LH chicane	Δx	35	mm
Bend angle of each LH chicane dipole	$\lvert\theta\rvert$	7.5	deg
Electron & IR beam size in LH (rms)	$\sigma_{x,y}$	180	μm
Nom. IR laser energy/pulse (0.25 nC)	E_{IR}	10	μJ
Nom. LH rms energy spread (0.25 nC)	σ_E	20	keV

Many laser heater system measurements were made during the 2009 commissioning and are described in detail in ref. [8]. The heater appears to damp the micro-bunching instability adequately, resulting in more FEL power when switched on, but it does not appear to completely remove a very small level of optical micro-bunching responsible for generating coherent OTR, compromising the quantitative use of the many OTR screens downstream of the first bunch compressor [9].

LINAC AND BUNCH COMPRESSORS

The *LCLS* linac includes two bunch compressor chicanes (BC1 & BC2), two non-compressing bend systems (DL1 & DL2), two transverse RF cavities (TCAV0 & TCAV3), and many diagnostics as shown in Figure 5. The linac RF and bunch compression parameters for a charge of 0.25 nC are listed in Table 3.

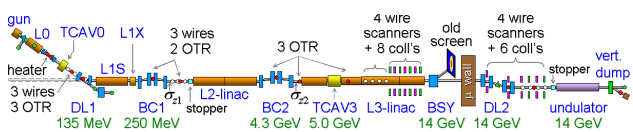

Figure 5: Linac layout from RF-gun to main dump. Red dots are OTR screens, green are YAG, and white are wire scanners.

The bunch compressors have been commissioned and the effects of coherent synchrotron radiation (CSR) in both have been measured, showing good agreement with respect to several computer codes [10]. Bunch lengths down to 2.5 μm rms (8 fs) have been measured.

Many feedback loops are now in operation, including RF-based loops and beam-based loops. The most

important loop uses 6 RF phases and amplitudes to control the energy at the four bend systems and the bunch length after each compressor (6 total measurements) [11]. The bunch length measurement is based on coherent edge radiation from the last dipole of each bunch compressor chicane [12] and each is calibrated in amperes of peak current with the transverse RF cavities. This critical "6×6" loop maintains the peak current after BC2 at 3 kA with a 5-Hz maximum rate (30 Hz beam rate), stabilizing the peak current to about 10% rms.

Eight older adjustable collimator jaw pairs near the end of the linac do primary beam collimation to protect the permanent magnet undulators [13], with six secondary collimators in front of the undulator (see below).

Table 3: Linac and bunch compression parameters at 0.25 nC. All phases (except laser) defined as $\varphi = 0$ at accelerating crest.

Parameter (RF crest at $\varphi = 0$)	**sym.**	**value**	**unit**
UV Laser Phase (2.856 GHz)	φ_L	–30	deg
L0 RF phase (2.856 GHz)	φ_0	–2	deg
L1S RF phase (2.856 GHz)	φ_1	–20	deg
L1X RF phase (11.424 GHz)	φ_x	–160	deg
L2 RF phase (2.856 GHz)	φ_2	–36	deg
L3 RF phase (2.856 GHz)	φ_3	0	deg
L1X RF voltage at crest phase	V_x	20	MV
BC1 momentum compaction	$R_{56\text{-}1}$	–45.5	mm
BC2 momentum compaction	$R_{56\text{-}2}$	–24.7	mm
Peak current before BC1	$I_{pk\text{-}0}$	33	A
Peak current after BC1	$I_{pk\text{-}1}$	250	A
Peak current after BC2	$I_{pk\text{-}2}$	3000	A
Total compression factor	C_1C_2	90	-

UNDULATOR SYSTEMS

The *LCLS* undulator is 132 m long (including breaks for quadrupole magnets) and is composed of thirty-three 3.4-m long planar, permanent magnet (Neodymium Iron Boron) undulator segments with 3-cm period, 6.8-mm full gap (fixed) height, and undulator parameter: $K = 3.5$. The vacuum chamber within each segment is highly polished aluminum (<0.2-μm surface finish) with a 5-mm height and 11-mm width. A 47-cm long break occurs between each undulator magnet, with each third break 90 cm long for future diagnostics. A quadrupole magnet, an X-band cavity-type high resolution beam position monitor (BPM) [14], a "beam-finder wire" (BFW), and flexible bellows is located at each break (see Figure 6 and Table 4).

One quadrupole (of 33, forming a weak FODO lattice) is located at the downstream end of each undulator, is independently powered, and also includes separately powered x and y steering coils. A cavity-type BPM is located 10 cm downstream of each quadrupole, each with <1 μm rms position resolution [14].

The BFW is an IN/OUT insertable cross-hair target located at the upstream end of each undulator with two 40-μm diameter carbon wires (see Figure 7). The wires are precisely fiducialized to the undulator magnetic center and are scanned in horizontal or vertical position, after insertion, by using the girder cam control. They are used to align the upstream end of the undulator to the beam, while the quadrupole and BPM are used to align the downstream end [15]. The 33 BFWs also measure x and y beam size at every break. The beam signal is taken from a Cherenkov monitor just downstream of the vertical dump bends where a thin metal window passes the degraded energy, over-bent electrons.

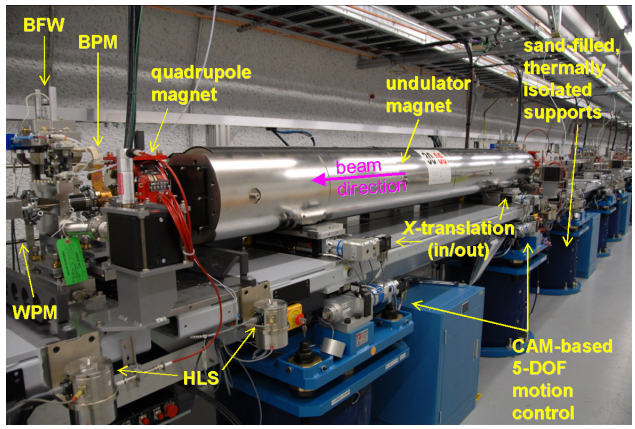

Figure 6: Photograph of one installed 3.4-m long undulator magnet on its motion-controlled girder with BPM, beam-finder wire (BFW), quadrupole magnet, wire-position monitor (WPM), hydrostatic leveling system (HLS), and horizontal translation stage for K adjustment and segment "in/out" control.

Table 4: *LCLS* Undulator and FEL Parameters at 1.5 Å.

Parameter (1.5 Å is at 13.6 GeV)	**sym.**	**value**	**unit**
Max. total undulator active length	L_u	112	m
Undulator parameter	K	3.5	-
Undulator peak field	B_y	1.25	T
Undulator period	λ_u	3.0	cm
Undulator pole gap (full height)	g_u	6.8	mm
Undulator gap cant angle	φ_u	5	mrad
Max. # of undulator segments	N_s	33	-
Undulator segment length	L_s	3.4	m
Quadrupole integrated gradient	GL_Q	±3.0	T
Measured BPM position resolution	$\sigma_{x,y}$	<0.5	μm
Mean beta function (1.5 Å)	$\langle\beta_{x,y}\rangle$	30	m

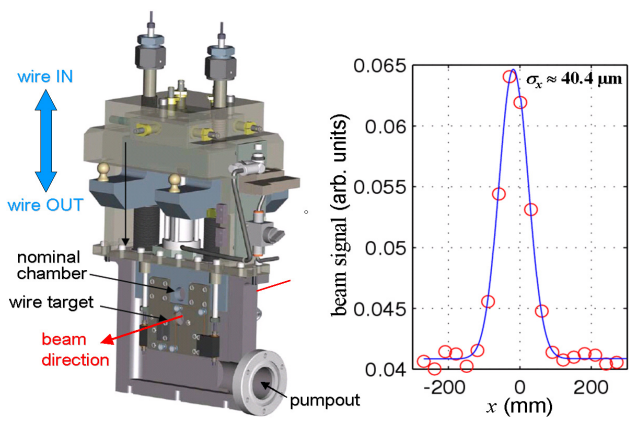

Figure 7: Beam Finder Wire (BFW) is used to align the upstream undulator end to the beam and also measure beam size.

The girder position control is accomplished with five motorized cams allowing remote motion control over five degrees of freedom: x and y position (at quadrupole, BPM, or BFW), plus pitch, yaw, and roll angles. Figure 8

shows the BPM-measured beam kicks as the quadrupole magnet position is changed horizontally in 0.5-μm steps. The high resolution BPMs downstream of the moved girder are used to detect the quadrupole motion and the BPMs upstream of the girder are used to correct for the incoming shot-to-shot trajectory jitter. The result, shown in Figure 8, shows 5-nrad resolution of a 30-nrad kick due to each 0.5-μm quadrupole position step and <1 μm of backlash. A 30-nrad kick at the quadrupole generates a 1-μm peak betatron oscillation in the undulator.

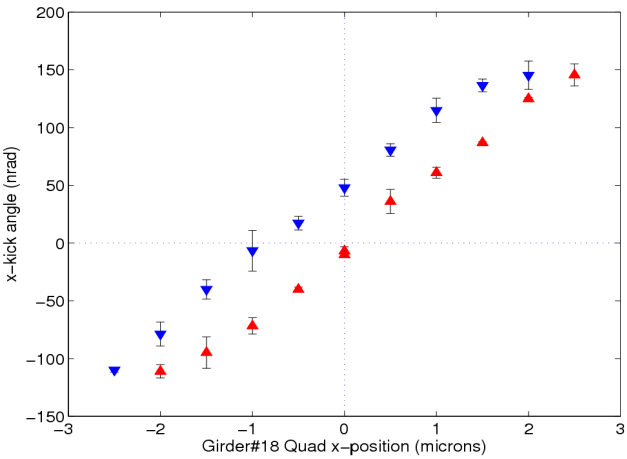

Figure 8: Measured backlash of girder showing <1 μm position control. The vertical axis is the x kick angle (nano-radians) at the quadrupole magnet seen on BPMs downstream of the girder. Red markers (▲) are positive x-steps and blue (▼) are negative.

The quadrupole magnet, BPM, BFW, vacuum chamber, and undulator segment are all mounted on the cam-controlled rigid girder. The beam can be steered using either quadrupole positions (typical) or weak steering coils (fast). In addition, the undulator magnet gap has a small cant angle (5 mrad) to allow remote tuning of K (±0.6%) by small horizontal translations of the undulator (±5 mm). Each undulator can also be fully displaced from the beam by 80 mm, to effectively switch that section off.

The final electron trajectory is established using beam-based alignment (BBA) [16], recording BPM readings for several different electron energies (from 4.3 to 13.6 GeV) while changing no settings within the undulator. This produces a dispersion-free trajectory over a wide energy range and establishes a very straight trajectory over the full undulator. The method appears to be quite successful so far, and a measurement is shown in Figure 9 plotting the x and y trajectories over the length of the undulator (132 m) with four very different input electron energies. The magnets upstream of the undulator are all scaled to each energy value in order to maintain focal lengths and bend angles, but no changes are made to any of the undulator system settings. The trajectory is highly dispersion-free.

The new long (340 m) transport line connecting the linac to undulator (LTU) was ready for beam in December 2008. This line (see Figure 5) includes six adjustable collimator jaw pairs (x, x', y, y', + 2 for $\Delta E/E$), four new x and y wire scanners for emittance and beta function measurements, a tune-up stopper in front of the undulator, and an abort kicker to quickly switch the beam out of the undulator when needed, while still keeping the full linac operating. The LTU also includes provisions for up to eight take-off points for future beams to new undulators.

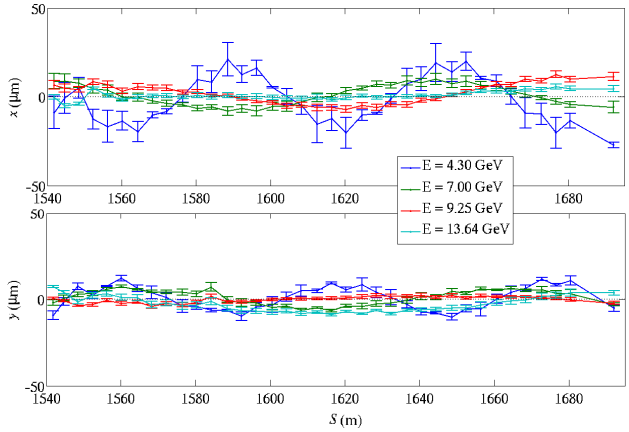

Figure 9: Undulator x (top) and y (bottom) trajectories at four different electron energies (4.3, 7.0, 9.25, and 13.6 GeV) showing the trajectory is highly dispersion-free and well aligned.

FEL LIGHT

The final phase of commissioning began in November 2008, with the undulator and long transport line from the linac commissioned through March 2. The *LCLS* was then shut down to install 21 undulator magnets on the existing undulator beamline, and for routine testing of safety interlocks. By April 7 the machine was running and the next 3 days were used to tune up the linac, establish undulator beam-based alignment, including BFW alignment, and also to measure the field integrals of each undulator when inserted.

Spontaneous radiation measurements for each undulator magnet were also made on a YAG screen using a Nickel foil to estimate the undulator parameter, K, for each section. (When the x-ray diagnostics are available, the K value for each undulator will be measured more precisely using a beam-based method with monochromator [17].)

On April 10, 2009 at 20:00, the first 12 undulator magnets were slowly inserted (slots 13-24 of 33 slots), trajectory corrections were applied for each, and by 21:00, after the peak current was raised back up to 3 kA, the first 1.5-Å FEL light was clearly observed (see Figure 10). It is especially remarkable, and encouraging for future 4th generation light sources, to see this hard-x-ray SASE FEL spring to life immediately at the very first trial, but of course also acknowledging the 2 years of commissioning work that went into the *LCLS* injector and accelerator performance prior to this first trial.

The relative FEL power is estimated for each shot by measuring the pixel sum on the YAG screen camera. The gain length is fitted by averaging 20-30 single shots on the YAG for each consecutively extracted undulator, one at a time, or by kicking the electron beam at each undulator consecutively to suppress the FEL gain past that point. Figure 11 shows a gain length measurement of 3.3 m with 25 undulators installed, a peak electron current of 3.0 kA, energy of 13.6 GeV (1.5 Å), and measured projected emittance values at the end of the linac of $\gamma\varepsilon_x \approx 1.2\ \mu$m, $\gamma\varepsilon_y \approx 0.7\ \mu$m. The time-sliced horizontal emittance is thought to be significantly smaller (see

Figure 3) than the projected measurement due to CSR effects in BC2 [10] and transverse wakefields in the main linac. The gain length is reasonably consistent with the electron beam parameters if the time-sliced emittance is assumed to be similar to that of Figure 3 (taken at 135 MeV) with 0.4 μm in each plane. The figure indicates SASE saturation at 1.5 Å in about 60 m, although small level of YAG saturation is likely at the highest power levels. At present, the YAG saturation is thought to be a small contribution to the saturation curve.

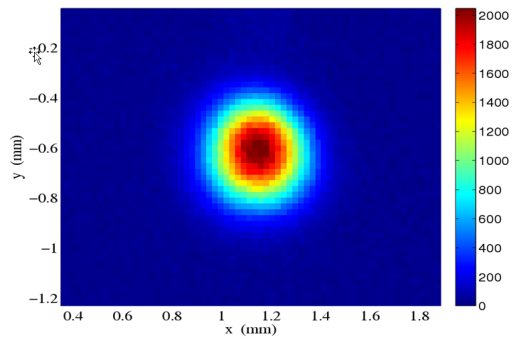

Figure 10: FEL x-rays at 1.5 Å on a YAG screen 50 m after the last inserted undulator (see Table 1 for measured parameters).

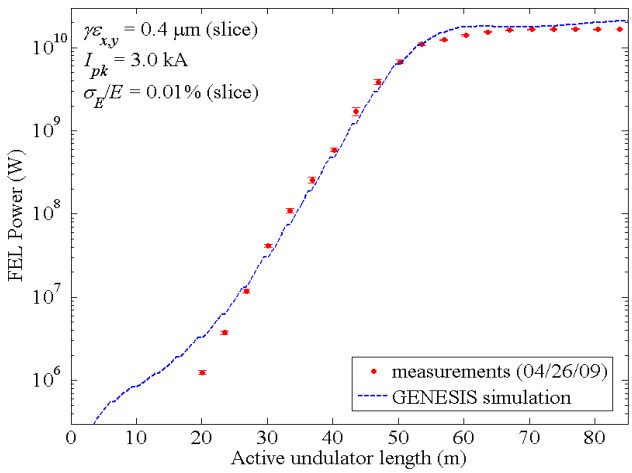

Figure 11: FEL power gain length measurement (red points) at 1.5 Å made by kicking the beam after each undulator sequentially. The measured gain length is 3.3 m and a *Genesis* simulation is overlaid in blue with e^- beam parameters shown. There are twenty-five 3.35-m long undulators installed here.

In order to estimate the energy in the x-ray pulse, we measure the electron energy loss across the undulator by varying the *K*-taper (*x*-position) over the full 70 m of undulator to vary the FEL power, and then measure the BPM *y*-position changes in the dump where the vertical dispersion is large. The incoming energy jitter is also subtracted. Figure 12 shows the YAG screen sum signal and the FEL-induced energy loss, both vs. the undulator *K*-taper (+1 mm corresponds to $\Delta K/K = -0.08\%$ over 70 m). The taper is optimal at about 1 mm and the FEL power is suppressed at –3 mm and +5 mm, revealing the peak electron energy loss due to the FEL process (4.6 MeV). At 0.25 nC this 4.6-MeV FEL-induced energy loss corresponds to 1.1 mJ, or about 0.8×10^{12} photons/pulse (15 GW of peak power for an estimated 75-fs full-width pulse length). If the FEL gain is suppressed by spoiling the emittance, this same taper scan shows no energy loss, demonstrating that the loss is associated with FEL power. These are preliminary measurements taken very recently with temporary diagnostics.

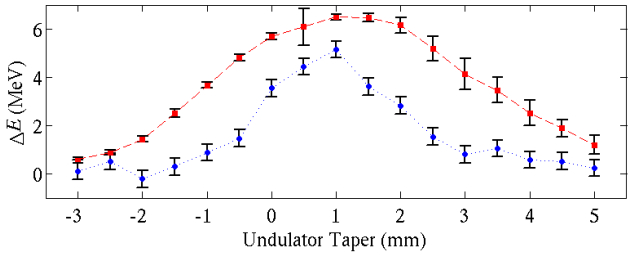

Figure 12: X-ray YAG screen sum signal on an arbitrary scale (red-dashed), and FEL energy loss in MeV (blue), both vs. undulator *K*-taper. The peak FEL energy loss is 4.6 MeV, which converts to 1.1 mJ of 1.5-Å x-ray energy per pulse.

SUMMARY

The *LCLS* has produced first FEL light and saturation at a wavelength of 1.5 Å with a 3.3-m gain length and up to 1.1 mJ in the x-ray pulse (0.8×10^{12} photons/pulse). The commissioning process has been remarkably successful, but is coming to a close in August when the first x-ray user operations are scheduled to start. The full 120-Hz operation will not begin until early 2010 and a full characterization of the x-ray beam is only possible when the x-ray diagnostics suite is ready for beam in June 2009.

ACKNOWLEDGEMENTS

It is a pleasure to acknowledge the contributions of Argonne National Laboratory's *LCLS* team, including design, fabrication, and testing of RF BPMs and undulator systems. We also thank the SLAC operations, controls, RF, engineering, metrology, and maintenance groups for their remarkable installation efforts and continuing support.

REFERENCES

[1] J. Arthur *et al.* SLAC-R-593, April 2002.
[2] R. Akre *et al.*, Phys. Rev. ST-AB **11**, 030703 (2008).
[3] R. Akre *et al.*, FEL'08, Gyeongju, Korea, 2008.
[4] R. Akre *et al.*, PAC'01, Chicago, IL, p. 2353, 2001.
[5] Y. Ding *et al.*, submitted to PRL, Jan. 2009.
[6] P. Emma *et al.*, PAC'05, Portland, OR, p. 344, 2005.
[7] Z. Huang *et al.*, Phys. Rev. ST-AB **7**, 074401 (2004).
[8] P. Emma *et al.*, these PAC'09 proceedings.
[9] H. Loos *et al.*, FEL'08, Gyeongju, Korea, 2008.
[10] K. Bane *et al.*, Phys. Rev. ST-AB **12**, 030704 (2009).
[11] J. Wu *et al.*, FEL'08, Gyeongju, Korea, 2008.
[12] H. Loos *et al.*, these PAC'09 proceedings.
[13] P. Emma, *et al.*, EPAC'06, Edinburgh, Scotland.
[14] S. Smith *et al.*, these PAC'09 proceedings.
[15] H.-D. Nuhn *et al.*, FEL'06, Berlin, Germany, 2006.
[16] P. Emma *et al.*, NIM **A** 429:407-413, 1999.
[17] J. Welch *et al.*, FEL'06, Berlin, Germany, 2006.